Pergamon

Int. J. Heat Mass Transfer. Vol. 41, Nos 4–5, pp. 709–718, 1998

Printed in Great Britain
0017–9310/98 $19.00+0.00

PII: S0017–9310(97)00164–6

Numerical analysis of electromagnetic wave in a partially loaded microwave applicator

S. TADA, R. ECHIGO and H. YOSHIDA

Department of Mechanical Engineering and Science, Faculty of Engineering, Tokyo Institute of Technology, 2-12-1 O-okayama, Meguro-ku, Tokyo 152, Japan

(*Received* 18 *October* 1996 *and in final form* 30 *May* 1997)

Abstract—A two-dimensional finite difference time domain method was employed to investigate the electromagnetic field in a microwave applicator filled partially with a dielectric material, operating in the dominant TE_{10} mode at a frequency of 2.45 GHz. The power distributions developed in the applicator and inside a lossy material are calculated. Results show correlations between the power absorption ratio and physical parameters, e.g. the position of the dielectric in the applicator and permittivities of the dielectric, which are dominant in the heating process. In particular, the energy absorption ratio strongly depends on the position of the dielectrics, which shows a sharp maximum when the dielectric is located around the middle of the applicator. In addition, power absorption ratios are calculated according to the definition newly proposed in this study, and they are compared with those obtained experimentally. © 1997 Elsevier Science Ltd.

1. INTRODUCTION

'Microwaves' is the generic name for electromagnetic (EM) waves having frequency in the range 10^9–10^{12} Hz or the characteristic wavelength range of 30 cm to 0.3 mm. The utilization of microwave power in heating technology over the past decade has become more widespread owing to their characteristics exhibited upon heating materials which contain water.

Generally, a high-frequency electric field causes polarization in a dielectric material. The motion of polarized charged particles lags behind the reversals of the electric field, leading to a power dissipation, i.e. the generation of heat. For water, the contribution of orientation polarization is extremely large when compared with those of any other materials; hence, heat is generated by the rotation and vibration of molecules possessing dipole structure. This is why microwave heating of water is highly efficient as well as rapid and direct.

Although, in principle, the microscopic or local heating mechanism by microwaves is simple, its macroscopic or overall mechanism reveals much greater complexity. The primary reason is that inherent difficulties in the treatment of the waveguide problems exist due to the complexity of the field distribution within the dielectric materials having the dimensions, on the same order as the wavelength. The secondary reason is that the dielectric properties such as the permittivity and the loss tangent vary strongly depending on temperature and materials. Consequently, even for a microwave oven, which is one of the most popular microwave applications, the detailed heating mechanism is not yet well known.

In order to obtain a basic understanding of the above-mentioned phenomena, the variations of power absorbed by a lossy material in a microwave waveguide are investigated numerically in the present study. We choose water as the dielectric material, since heating materials which contain free water or bound water are the subject of a vast number of studies in various domains.

A two-dimensional numerical analysis is conducted to clearly describe electromagnetic interferences and power absorption in the dielectric inserted in the waveguide. In the calculation, wave distributions that directly affect the energy absorbed by the dielectric are obtained for various permittivities and positions of the dielectric. Furthermore, calculated energy absorption ratios for various permittivities and positions of the dielectric are compared with the experimental results corresponding to the analysis, and a detailed discussion concerning the mechanism of microwave heating is given.

2. NUMERICAL ANALYSIS

In principle, the analysis of the EM field can be settled by solving the simultaneous partial differential equations given by Maxwell. In the past, the scalar wave analysis using the Helmholtz equation or the Heltz vector [1, 2] the vector wave analysis [3, 4] were frequently applied to the microwave-material interaction problems.

Recently, the finite-difference time-domain (FDTD) method [5] has been used to provide the temporal and spatial variation of EM fields, which are effective for predicting much more accurate influences of processing parameters, such as the dielectric

NOMENCLATURE

A	surface area [m^2]
a	spanwise length of the applicator [m]
b	height of the applicator [m]
c	light velocity [$m\ s^{-1}$]
D_p	penetration depth [m]
$\mathbf{E}$	electric field vector [$V\ m^{-1}$]
$\mathbf{H}$	magnetic field vector [$A\ m^{-1}$]
j	imaginary unit
k_z	z component of wave vector [m^{-1}]
k	attenuation constant
l	length of the applicator [m]
n	refractive index
P	time average of energy density per unit volume of waveguide [$W\ m^{-3}$]
P_{ra}	energy absorption ratio
p	local energy density [$W\ m^{-3}$]
$\mathbf{P}_e$	energy density flux vector of reflected wave [$W\ m^{-2}$]
$\mathbf{P}_i$	energy density flux vector of forward wave [$W\ m^{-2}$]
$\mathbf{r}$	positional vector [m]
$\mathbf{S}$	Poynting vector of electromagnetic waves [$W\ m^{-2}$]
T	temperature [K]
t	time [s]
$\tan\delta$	loss tangent ($=\varepsilon''_{eff}/\varepsilon'$)
$\mathbf{u}$	group velocity vector [$m\ s^{-1}$]
V, v	volume of dielectric [m^3]
x, y, z	Cartesian coordinates [m]
Z	characteristic impedance [Ω]
z_d	position of the dielectric center [m].

Greek symbols

ε	permittivity [$F\ m^{-1}$]
ε''_{eff}	effective loss factor
ε_r	relative permittivity
ΔP	absorbed energy [W]
Γ	heat capacity [$J\ K^{-1}$]
λ_c	cutoff wavelength [m]
λ_f	free-space wavelength [m]
λ_g	waveguide wavelength [m]
μ	permeability [$H\ m^{-1}$]
σ	electric conductivity [$S\ m^{-1}$]
τ	cycle period of electromagnetic waves [s]
ω	angular frequency [$rad\ s^{-1}$].

Subscripts

A	amplitude
all	applicator
di	dielectric
x, y, z	coordinates
0	vacuum.

Superscripts

¯	time average
~	complex value
*	dimensionless value
′	real part
″	imaginary part.

position, shape, and permittivity, on the microwave heating mechanism.

The FDTD method has received much attention due to its versatility in handling objects with complex shapes and easy development of mathematical descriptions. Discussions on applying the FDTD method to microwave radiation problems are found in Refs [6, 7], particularly microwave heating of samples with constant physical properties and material processings.

The present analysis aims for the calculation of the energy flux of microwaves and the time evolution of the energy density within the lossy dielectric waveguide, using Maxwell's equations of the FDTD formulation based on the computer algorithm established by Yee [5]. As mentioned above, dielectric position, shape, and physical properties with respect to the microwave applicator geometries are dominant over the development of wave patterns which directly affect the efficiency of microwave energy absorption in dielectrics. Therefore, by focusing on the effects of the variation of permittivity and the position of the dielectric on wave patterns, the influences of EM field variation on microwave energy absorbed in the dielectric is primarily examined.

2.1. *Electromagnetic field within waveguide*

In the present analysis, frequency dispersion due to the rapidly varying magnetic field does not occur in the materials, so the permeability of the dielectric material is assumed to be that in vacuum. As shown in Fig. 1, we assume that a monochromatic wave of

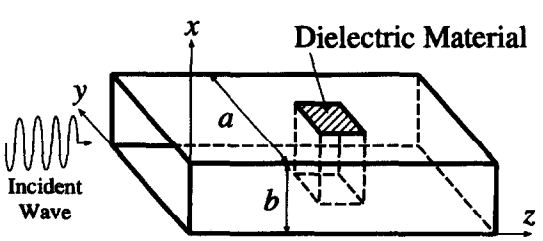

Fig. 1. Schematic of the microwave applicator and coordinate system.

TE_{mn} mode transmits through a rectangular waveguide of inner dimensions $a \times b$. The suffixes m and n indicate the number of half-sinuosoids of variation of the E field along the x- and y-axes, respectively. The waveguide is assumed to be perfectly conducting.

The boundary conditions for the TE_{mn} wave are formulated as follows:

- For the surface of the conducting wall, from Faraday's law and Gauss's theorem

$$\mathbf{E}_{\parallel} = 0, \mathbf{H}_{\perp} = 0. \tag{1}$$

- For the interface between air and dielectric material, from Ampére's law and Gauss' theorem

$$\mathrm{rot}\,\mathbf{H}_{\parallel} = \mathrm{rot}\,\mathbf{H}_{\mathrm{di}\parallel}, \mathbf{H}_{\perp} = \mathbf{H}_{\mathrm{di}\perp}, \tag{2}$$

where the subscript di denotes dependant variables in the dielectric material.

The cutoff wavelength of the propagating TE_{mn} wave is

$$\lambda_c = \frac{1}{\sqrt{(m/2a)^2 + (n/2b)^2}} \quad (m, n = 0, 1, 2, \ldots; m+n \geqslant 1). \tag{3}$$

From eqn (3) and the definition of microwave wavelength in free space

$$\lambda_f = \frac{2\pi}{\omega}\sqrt{\frac{1}{\varepsilon_0 \mu_0}} \tag{4}$$

the waveguide wavelength λ_g of microwaves is solved as

$$\lambda_g = \lambda_f / \sqrt{1 - (\lambda_f/\lambda_c)^2}. \tag{5}$$

The group velocity u_z of microwaves is

$$u_z = \frac{\partial \omega}{\partial k_z} = \frac{2k_z}{2\omega\varepsilon\mu - j\mu\sigma}. \tag{6}$$

The characteristic impedance becomes

$$Z = \sqrt{\frac{\mu_0}{\varepsilon_0}} = 376.73\,[\Omega]. \tag{7}$$

2.2. *Objective of the analysis and method*

We assume that microwaves of 2.45 GHz transmit through a brass waveguide with inner dimensions of 109.22 mm (width) × 54.61 mm (height). The power loss in the waveguide wall is ignored. The analytical approach, which starts by separating variables, leads to the following field equations after considering the boundary conditions specified by eqns (1) and (2) for the fundamental TE_{10} mode:

$$E_y = E_z = H_x = 0. \tag{8}$$

The TE_{10} mode is the lowest mode of the supported microwave field for waves transmitted in the present rectangular waveguide without power dissipation. The type of wave mode is prescribed by the frequency and the waveguide dimensions. Therefore, from eqn (3), the relevant cutoff wavelength is obtained as

$$\lambda_c = 2a = 218.44\,[\mathrm{mm}]. \tag{9}$$

From eqns (4), (5) and (9), λ_f and λ_g are

$$\lambda_f = 122.36\,[\mathrm{mm}], \lambda_g = 147.72\,[\mathrm{mm}]. \tag{10}$$

Since the TE_{10} mode has no variation of field in the direction between the broad faces, a two-dimensional numerical calculation over the y–z plane in Fig. 1 is applicable to the analysis under consideration. We define dimensionless quantities as

$$\mathbf{E}^* = \frac{\mathbf{E}}{E_{Ax}}, \quad \mathbf{H}^* = \frac{Z\mathbf{H}}{E_{Ax}}, \quad \mathbf{r}^* = \frac{\mathbf{r}}{\lambda_g}, \quad t^* = \frac{ct}{\lambda_g} \tag{11}$$

where the superscript * represents the dimensionless quantity.

Considering eqn (8), Maxwell's equations are expressed in dimensionless form as

$$\frac{\partial E_x^*}{\partial z^*} = -\frac{\partial H_y^*}{\partial t^*} \tag{12}$$

$$\frac{\partial E_x^*}{\partial y^*} = \frac{\partial H_z^*}{\partial t^*} \tag{13}$$

$$\frac{\partial H_z^*}{\partial y^*} - \frac{\partial H_y^*}{\partial z^*} = Z\lambda_g \sigma E_x^* + \tilde{\varepsilon}_r \frac{\partial E_x^*}{\partial t^*} \tag{14}$$

where $\tilde{\varepsilon}_r = \varepsilon_r' - j\varepsilon_r''(= (n - jk)^2)$.

The spatial terms and the temporal terms in these equations are approximated using finite difference equations for E and H fields. Spatially, as shown in Fig. 2, eqns (12)–(14) are solved on a staggered grid system, and temporally they are solved alternately for both the electric and magnetic fields. Furthermore, in order to automatically satisfy the boundary condition for the surface of the waveguide and of the dielectric, grid points of E_x are arranged so that grid points on computational boundaries are distributed along physical boundaries.

The *dynamic* boundary condition for the alternative

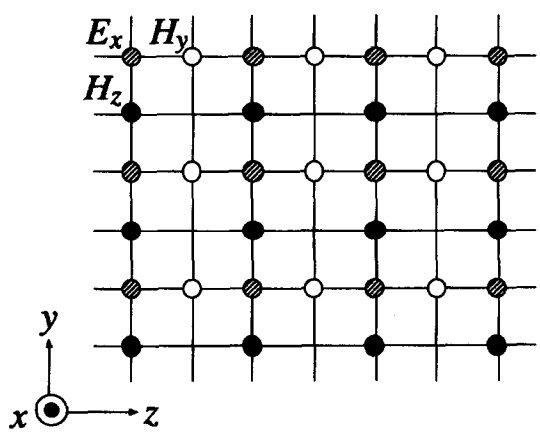

Fig. 2. Staggered grid configuration.

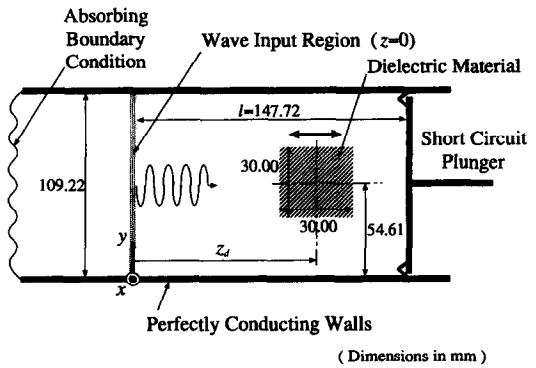

Fig. 3. Cross-sectional view of the microwave applicator (top view).

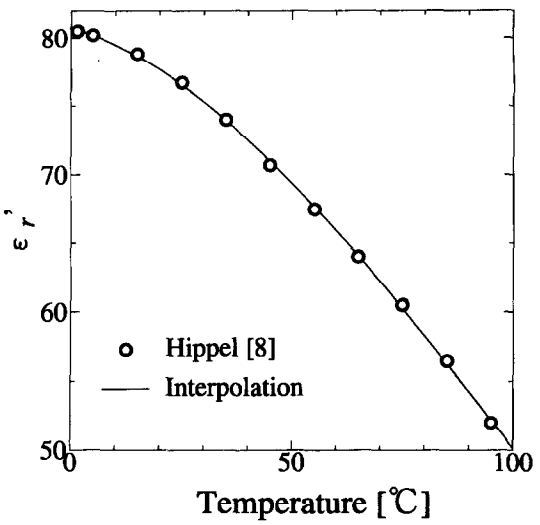

Fig. 4. Dependence of the relative permittivity of water on temperature.

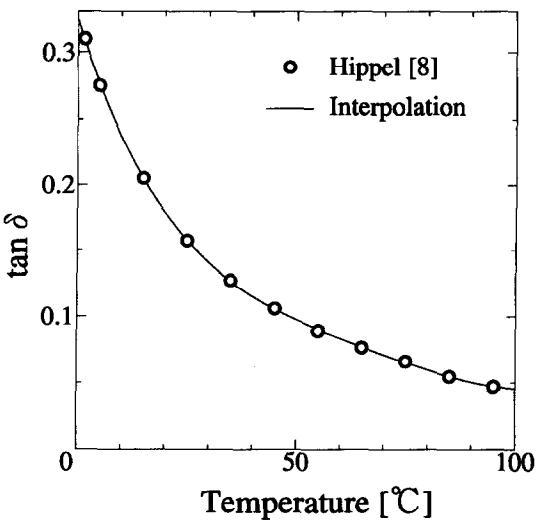

Fig. 5. Dependence of the loss tangent of water on temperature.

EM field over the cross section at $z = 0$ (wave input region), as shown in Fig. 3, gives the electric field of the incident plane monochromatic wave

$$E_x = E_{Ax} \sin\left(\frac{y}{\lambda_c} 2\pi\right) \cdot \exp\left(\frac{z - ct}{\lambda_f} 2j\pi\right). \quad (15)$$

The standing wave varies sinusoidally with time, and also with the position along the waveguide; therefore, the distance between the input region ($z = 0$) of the microwave and the plunger face is taken to be an integer multiple of wavelengths $n \cdot \lambda_g$ ($n = 1, 2, \ldots$).

For the reflected wave which reaches the *dynamic* boundary of the computational region, i.e. the left-hand end of the waveguide shown in Fig. 3, an absorbing boundary condition

$$\frac{\partial \mathbf{E}}{\partial t} - \mathbf{u} \frac{\partial \mathbf{E}}{\partial \mathbf{r}} = 0 \quad (16)$$

is adopted. Here, $\mathbf{u}$ is the group velocity vector of microwaves, and it provides the z-axis component expressed by eqn (6).

Water is selected as the workload of the guided wave. Since the relative permittivity ε_r' and the dielectric loss angle $\tan\delta (= \varepsilon_{r_{eff}}''/\varepsilon_r')$ of water change considerably depending on the temperature, in the present study, ε_r and $\tan\delta$ are given as

$$\varepsilon_r(T) = \sum_n a_n T^n, \tan\delta(T) = \sum_n b_n T^n \quad (17)$$

to take into account the influence of temperature on the energy absorption ratio precisely. Where ε_{eff}'' is the effective loss factor denoted as:

$$\varepsilon_{eff}''(\omega) = \varepsilon''(\omega) + \frac{\sigma}{\omega}. \quad (18)$$

Measured data [8] are used to determine the coefficients a_n and b_n. The temperature dependence of ε_r' and $\tan\delta$ are shown in Figs 4 and 5, respectively.

3. RESULTS AND DISCUSSION

3.1. *Analytical conditions*

A two-dimensional numerical analysis of the microwave applicator with a spanwise length $a = 109.22$ mm and length $l = 147.72$ mm ($= \lambda_g$) is performed. The cross-sectional shape of the dielectric material inserted in the waveguide is square with dimensions 30.00×30.00 mm. The dielectric is moved along the center axis of the applicator $y^* = 0.37$ ($y = 54.61$ mm), within the range z_d^* ($= z_d/\lambda_g$) $= 0.2$–0.9 ($z_d = 29.54$–132.95 mm).

The calculation conditions are as follows:

- time step: $\Delta t = 2.01$ ps,
- grid size: $\Delta y = \Delta z = 1.00$ mm,

• number of grids: $M = 149$ (length) $\times$ 110 (width).

The conversion criteria is given by

$$\max\left(\sum_{m,n} R_{E_x}, \sum_{m,n} R_{H_y}, \sum_{m,n} R_{H_z}\right) < 10^{-4} \qquad (19)$$

where

$$R_\phi = \left|\frac{\phi^N_{m,n} - \phi^{N-1}_{m,n}}{M\phi^N_{m,n}}\right| \qquad (20)$$

is the relative residual of the quantity ϕ on the nodal point (m, n) at the Nth cycle. The amplitude of electric field E_{Ax} in eqn (15) is set to $E_{Ax} = 1.00$ V m^{-1}. For the permittivity and permeability of air, those of vacuum are used.

3.2. *Electric field distribution*

In the beginning, to understand the detailed structures of electric fields developed inside the applicator, the numerical analysis of the following three cases are conducted:

(1) Waveguide is empty and its dielectric constant is unity (which corresponds to that of air).
(2) Waveguide is partially filled with transparent medium with finite dielectric constant.
(3) Waveguide is partially filled with absorbing medium.

To simplify the following discussion, positions of dielectrics are fixed at $z^*_d = 0.60$ ($z_d = 88.63$ mm) for both Cases 2 and 3. For relative permittivities, values of water at 20°C, i.e. $\varepsilon'_r = 78.55$ and $\varepsilon''_{r_{eff}} = 13.85$, obtained using eqn (17) are used. Results are shown in Figs 6–8. In the figures, vertical axes represent the intensity of electric field E_x, which is normalized to the amplitude of the input EM wave, E_{Ax}.

Figure 6 shows the standing wave of the first mode, TE_{10}, in the applicator (Case 1). The figure shows the moment when the electric field attains its maximum. A standing wave is formed by superimposition of the forward wave propagated from the inlet $z^* = 0$ and of the reflected wave from the plunger end $z^* = 1.0$ ($z = 147.72$ mm).

When a dielectric is inserted in the waveguide where

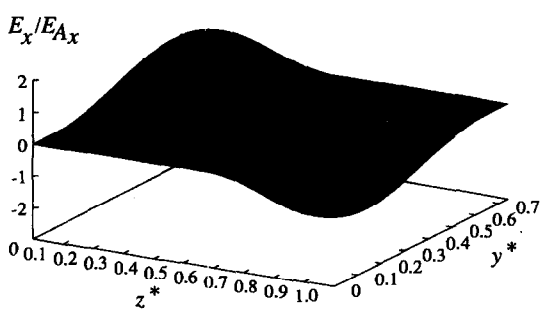

Fig. 6. Distribution of the electric field (Case 1: $\varepsilon'_r = 1, \varepsilon''_{r_{eff}} = 0$).

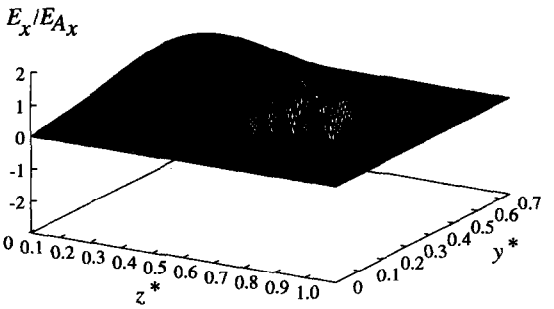

Fig. 7. Distribution of the electric field (Case 2: $\varepsilon'_r = 78.55, \varepsilon''_{r_{eff}} = 0$).

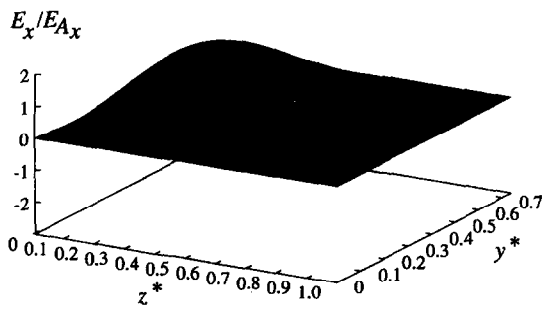

Fig. 8. Distribution of the electric field (Case 3: $\varepsilon'_r = 78.55, \varepsilon''_{r_{eff}} = 13.85$).

the developed standing wave shown in Fig. 6 is formed, the refractive index of the microwave over the dielectric surface varies accompanied with the variation of the field intensity within the dielectric. This leads to a drastic deformation of the field pattern throughout the waveguide, as shown in Fig. 7. The electric field is concentrated within the dielectric so that the electric field which surrounds the dielectric is weakened. Furthermore, focusing attention on the dielectric, a complex field distribution associated with many nodes and antinodes is formed by interference between the forward wave and waves reflected at the side walls and at the plunger end. Consequently, a new wave pattern which satisfies the new boundary condition over the dielectric surface is established. In addition, the electric field distribution shows a striking contrast between inside and outside the dielectric, since the apparent field intensity in the dielectric varies considerably; it is increased to a value two orders of magnitude greater than the field intensity exhibited outside the dielectric.

Figure 8 shows the wave distribution of the electric field when an absorbing material is inserted in the waveguide (Case 3). The relative permittivities of the material are $\varepsilon'_r = 78.55$ and $\varepsilon''_{r_{eff}} = 13.85$, which correspond to those of water with 20°C. Within the dielectric, the electric field attenuates owing to energy absorption, and thereafter the absorbed energy is converted to the thermal energy, which increases the water temperature. In the figure, the electric field within the

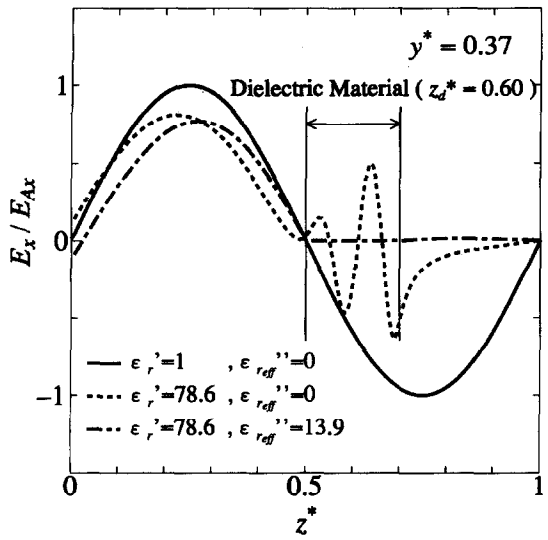

Fig. 9. Electric field strength along the center axis of the applicator for various relative permittivities.

dielectric is almost extinguished while the field pattern outside the dielectric keeps almost the same shape as that of Case 1. The existence of the dielectric has a fairly small influence on the electric field in the left-hand half of the waveguide.

Figure 9 shows the electric field distribution for Cases 1–3, along with the center axis $y^* = 0.37$ ($y = 54.61$ mm) of the applicator. All of them are normalized with respect to the amplitude of the field for Case 1. A large difference in the wave pattern is observed on changing the type of dielectric. However, as a common feature, the dielectric strongly affects the field patterns, i.e. intensity of the field around the dielectric is considerably weakened regardless of the type of dielectric inserted in the waveguide (whether it is the transparent material or absorbing one). In particular, when the absorbing material is inserted in the waveguide, EM waves near the plunger are almost extinguished.

As an interesting feature obtained in the numerical analysis, the amplitude of the waves developed in the absorbing materials widely changes for various $\varepsilon''_{r_{eff}}$. The amplitude of the wave inside the absorbing materials decreases with increasing $\varepsilon''_{r_{eff}}$. On the other hand, the variations of the phase or the variations of the wavelength are hardly observed.

Now let us proceed with a detailed discussion on the electric field of Case 3. The penetration depth D_p of water at 20°C is approximately $D_p = 15$–25 mm according to both the theoretical value

$$D_p = 1 \Big/ \omega \sqrt{\frac{\varepsilon\mu}{2}\left[\sqrt{1+\left(\frac{\sigma}{\omega\varepsilon}\right)^2}-1\right]} \qquad (21)$$

and the measured value [9].

From the definition of the penetration depth D_p, the electric field intensity in the dielectric falls to approximately $1/e$ of its strength with distance D_p from the dielectric surface. Nevertheless, as shown in Fig. 9, in contrast to this, the electric field within the dielectric is almost extinguished with distance less than the evaluated $D_p^* = 0.1$–0.17 ($D_p = 15$–25 mm) from the surface of the dielectric. This is because the strength of microwaves has sufficiently weakened owing to the interference among the incident wave and reflected waves before the microwaves penetrate the dielectric. Accordingly, these microwaves are further weakened after passing into the dielectric. On the basis of these findings, the 'penetration depth' does not adequately explain the influence of the geometry and the position of dielectric. A similar discussion is also given in Ref. [7].

Next, to examine the influence of the position of the dielectric on the wave distribution, additional calculations for Case 2 are performed by changing the dielectric position stepwise along the center axis. Figure 10 shows the wave distribution along the center axis for three dielectric positions. As noted before, the dielectric used in Case 2 is a transparent material, and the relative permittivities are $\varepsilon'_r = 69.5$ and $\varepsilon''_{r_{eff}} = 0$. The value of $\varepsilon'_r = 69.5$ corresponds to that of water at 50°C. When the dielectric is located in the middle of the applicator $z_d^* = 0.5$ ($z_d = 73.86$ mm), the field strength both inside and outside the dielectric is rather strong. However, when the dielectric is moved to the left, 14.77 mm from the middle point, $z_d^* = 0.4$ ($z_d = 59.09$ mm), the wave pattern is drastically changed. The strength of the wave is considerably weakened throughout the applicator. In addition, the standing wave is extinguished in the right-hand half of the applicator. When the dielectric is located further away from the center, $z_d^* = 0.3$ ($z_d = 44.32$ mm), the standing wave is also extinguished in the right-hand side of the dielectric, and the polarity of the electric

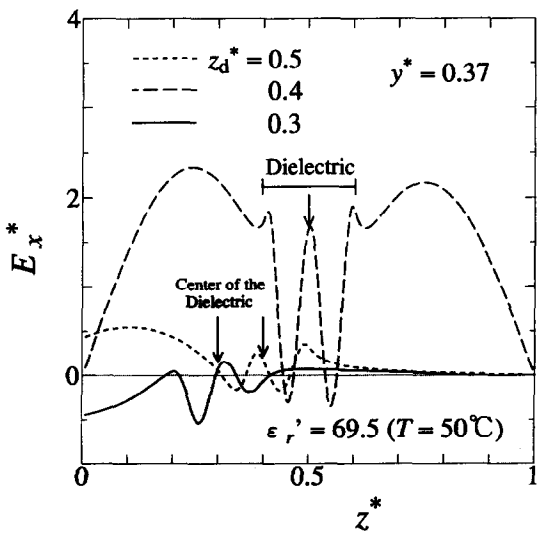

Fig. 10. Electric field strength along the center axis of the applicator for various dielectric positions ($\varepsilon''_{r_{eff}} = 0$).

field in the left-hand side and that in the right-hand side are reversed.

3.3. *Energy density variation*

In this section, energy density is calculated in order to examine the dependence of the energy density within dielectrics on position of the dielectric for various values of relative permittivities. For simplicity, dielectrics are chosen as transparent materials.

The energy density of electric fields are proportional to the square of the electric field as:

$$p \sim |\mathbf{E}|^2. \tag{22}$$

Therefore, by integrating eqn (22) over the whole area of the dielectric and the period of one cycle of the field variation, we define the time average of the energy density within the dielectric as:

$$P_{\mathrm{di}} \sim \frac{1}{\tau V}\int_0^{\tau}\int_{V_{\mathrm{di}}} |\mathbf{E}|^2 \,\mathrm{d}v\,\mathrm{d}t \tag{23}$$

where V_{di} is the volume per unit height of the dielectric and τ is the cycle period of the alternating field. Time average of the energy density within the applicator also can be defined in the same way as:

$$P_{\mathrm{all}} \sim \frac{1}{\tau V}\int_0^{\tau}\int_{V_{\mathrm{ap}}} |\mathbf{E}|^2 \,\mathrm{d}v\,\mathrm{d}t \tag{24}$$

where V_{ap} is the volume per unit height of the applicator and τ is the cycle period of the alternating field.

Figure 11 shows the variations of $P_{\mathrm{di}}/P_{\mathrm{all}}$ with the position of the dielectric, z_{d}^*. $P_{\mathrm{di}}/P_{\mathrm{all}}$ is the ratio of the time average of the energy density in the dielectric, P_{di}, to that of the whole volume of the applicator, P_{all}. $P_{\mathrm{di}}/P_{\mathrm{all}}$ changes markedly with the variation of the dielectric position, and the position of the maximum $P_{\mathrm{di}}/P_{\mathrm{all}}$ varies with the variation of $\varepsilon_{\mathrm{r}}'$. The maximum $P_{\mathrm{di}}/P_{\mathrm{all}}$ increases with decreasing $\varepsilon_{\mathrm{r}}'$ while with decreasing $\varepsilon_{\mathrm{r}}'$, the dielectric position where $P_{\mathrm{di}}/P_{\mathrm{all}}$ attains a maximum move away from the plunger end ($z^* = 1.00$). In particular, almost all of the energy of the input microwaves concentrates within the dielectric when the position of the dielectric in the waveguide is chosen properly.

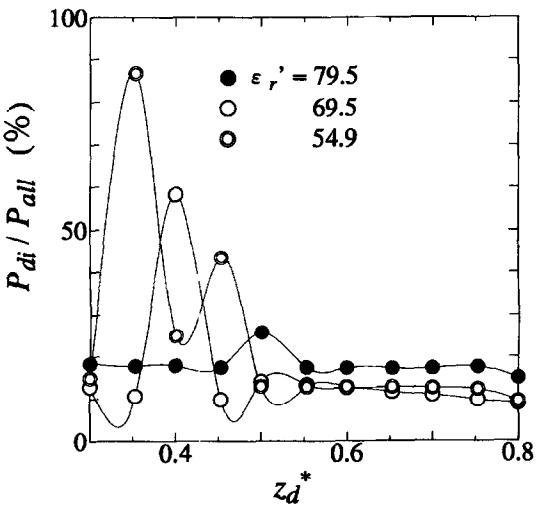

Fig. 11. Dependence of energy density ratio on positions of the dielectric for various relative permittivities ($\varepsilon_{\mathrm{r_{eff}}}'' = 0$).

3.4. *Comparison of experiment and numerical analysis*

Prior to comparing the results of the experiment and those of the analysis, it is necessary to introduce the description of the energy absorption ratio using values provided by the present calculation. For absorbing materials, the energy balance within the applicator is

$$\Gamma\frac{\mathrm{d}T}{\mathrm{d}t} = \frac{1}{2}\omega\varepsilon_0\int_V \varepsilon_{\mathrm{r_{eff}}}''|\mathbf{E}|^2\,\mathrm{d}v = \frac{1}{\tau}\oint_A\int_0^{\tau}(\mathbf{P}_{\mathrm{i}}-\mathbf{P}_{\mathrm{e}})\,\mathrm{d}t\cdot\mathrm{d}\mathbf{A} \tag{25}$$

where Γ is the heat capacity of the dielectric, $\mathrm{d}T/\mathrm{d}t$ is the rate of temperature increase by absorption of microwave energy, $\mathbf{P}_{\mathrm{i}}$ is the energy density flux vector of the forward wave, and $\mathbf{P}_{\mathrm{e}}$ is the energy density flux vector of the reflected wave. Here, the surface is integrated with respect to the wave input surface of the applicator $z = 0$ in Fig. 3.

The relationship between the inlet energy density flux P_{i} and the time average of the Poynting vector $\bar{\mathbf{S}}$ is

$$\frac{1}{\tau}\int_0^{\tau}\mathbf{P}_{\mathrm{i}}\,\mathrm{d}t = \bar{\mathbf{S}}. \tag{26}$$

Using this, the energy absorption ratio P_{ra} is defined as

$$P_{\mathrm{ra}} = \frac{\Gamma}{\oint\bar{\mathbf{S}}\,\mathrm{d}\mathbf{A}}\cdot\frac{\mathrm{d}T}{\mathrm{d}t}. \tag{27}$$

In the experiment, energy absorption ratios are calculated by measuring temperature increases for water and the amount of absorbed microwave energy indicated by a power monitor connected to the microwave power equipment. On the other hand, in the analysis, energy absorption ratios are calculated by substituting the second equation on the right-hand side of eqn (25) into eqn (27). Here, $\mathbf{P}_{\mathrm{i}}$ and $\mathbf{P}_{\mathrm{e}}$ are obtained numerically.

Instrumentation is diagrammatically shown in Fig. 12. Microwaves with a frequency of 2.45 GHz generated by a magnetron source are introduced into the waveguide (109.22 mm in spanwise, 54.61 mm in height); then after passing through the constituent items, they are reflected by the plunger which is installed at the end of waveguide. The reflected microwaves, attenuated due to energy absorption by water, are converted into thermal energy by the isolator; thereafter, they are released to the outside. The effects

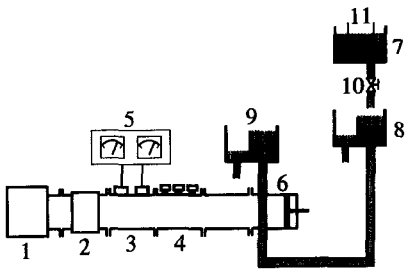

1. Generator 2. Isolator 3. Dual Directional Coupler
4. Three Stubs Tuner 5. Power Monitor 6. Applicator
7. Main Tank 8. Overflow Tank A 9. Overflow Tank B
10. Ball Valve 11. Heater

Fig. 12. Instrumental setup.

of any mismatch will not be canceled so that the experiment is carried out in the EM field where TE_{10} mode is dominant.

The dimensions of the applicator are 109.22 mm in spanwise, 54.61 mm in height and 260.0 mm in length. As the applicator is made of a drawn-on-mandrel brass rectangular tube, the disturbance and the losses of EM field due to the division of current flows in the wall are sufficiently small; hence the power losses in waveguide walls are negligible. In addition, a square brass tube is soldered on upper and lower sides of the waveguide to introduce the water duct into the waveguide. The inner dimensions of the corresponding square tube are 30×30 mm, providing 60 mm cutoff wavelength. On the other hand, the microwaves of the wavelength 147.72 mm which is larger than that of the tube's cutoff cannot propagate along the corresponding square tube; therefore, the effect of heating in the square tube is almost negligible.

The portion of the flow duct exposed to microwave irradiation (inside the waveguide) is a tube with outer dimensions 30×30 mm square, made of anhydrous quartz plates with 0.05 loss factor. In addition, Pyrex circular tubes are connected to both ends of the quartz tube. Water passing through the tube is almost uniformly heated, since, as shown in the numerical results, the standing wave with several number of antinodes is generated within the duct during microwave irradiation.

The flow duct is covered with an additional layer of glass fiber to reduce the heat losses to a minimum. However, the portion of the flow duct inside the applicator is not insulated since any insulating material absorbs microwave energy and disturbs the EM field developed in the waveguide. The applicator is flanged to the Three Stubs Tuner while the other end of the applicator is short-circuited by the plunger. The short-circuited plunger inside the applicator is adjustable to provide a variable distance between the center axis of the quartz tube and the plunger's front surface, from 35 to 140 mm. The length of '140 mm' approximately corresponds to three quarters of the guided wavelength.

Figures 13–15 show the energy absorption ratio P_{ra} of water obtained using eqn (27), accompanied by the corresponding experimental result, for three values of permittivity. In the experiment, the water flows through a rectangular quartz tube of thickness 1 mm. However, the tube wall is not taken into account in the calculation since the tube wall thickness of 1 mm is the dimension corresponding to only one mesh resolution of the numerical grid system.

The discrepancies in positions of the minimum P_{ra} between the experiment and analysis mainly result from the high sensitivity of EM fields. As discussed previously for the analytical results, the refractive

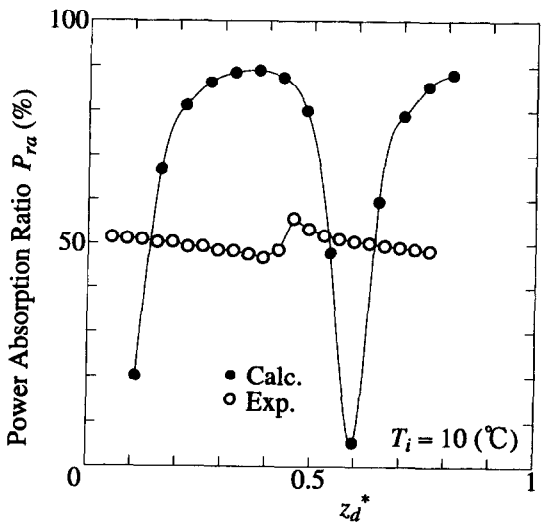

Fig. 13. Variation of power absorption ratio with position of the dielectric (water temperature 10°C).

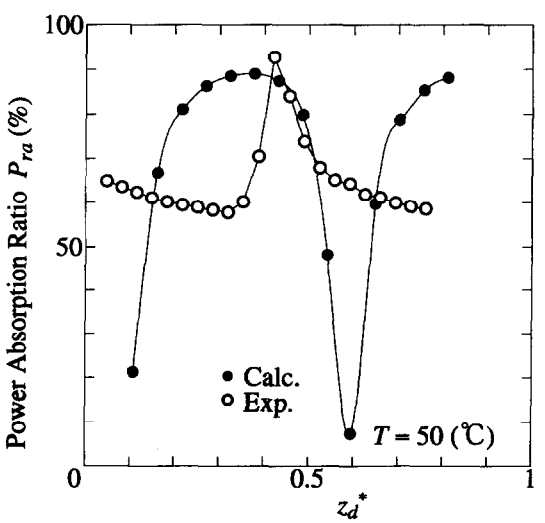

Fig. 14. Variation of power absorption ratio with position of the dielectric (water temperature 50°C).

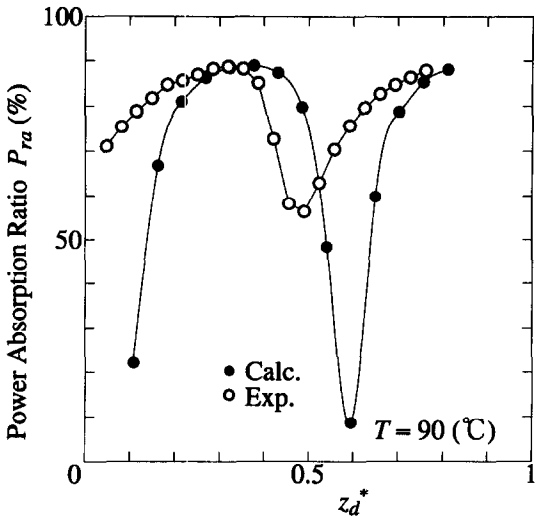

Fig. 15. Variation of power absorption ratio with position of the dielectric (water temperature 90°C).

index at the interface between the dielectric and air changes drastically with the dielectric position, especially near the middle of the waveguide. Therefore, a small change in the position of the dielectric near the middle causes a considerable variation in the wave pattern, leading to a marked change in P_{ra}. In addition, in contrast to the strong dependence of the dielectric position of P_{ra}, a change in the water temperature has no appreciable effect on the energy absorption ratio. P_{ra} changes gradually with respect to the change of the water temperature. On the other hand, experimental results show strong dependencies of temperature on P_{ra} as well as the dependence on the dielectric position. The results of the analysis for water at 90°C shown in Fig. 15 is similar to the corresponding experimental result with the exception of the minimum value of P_{ra}.

4. CONCLUSIONS

In the present study, the influences of the position and permittivity of dielectric material in a microwave applicator on the energy absorption ratio of the dielectric were investigated numerically. In the numerical analysis, Maxwell's equations were solved by employing Yee's formulation, detecting wave distributions and energy densities established in the waveguide during microwave irradiation. Furthermore, results are compared with the experimental results for water flowing through a rectangular duct installed in the 2.45 GHz microwave applicator. The following knowledge concerning the microwave heating mechanism is obtained.

(1) The standing wave of the electromagnetic field formed in the applicator is concentrated inside the dielectric material when the dielectric material is inserted in the applicator. At that time, a standing wave with many nodes and antinodes is formed within the materials.
(2) A marked increase in the energy absorption ratio can be obtained when the dielectric is placed at or around the middle of the applicator, where a node of the standing wave is formed when dielectric materials do not exist.
(3) The electric field intensity inside the material varies considerably with variation of the permittivity and its distance from the end of the waveguide plunger.
(4) When the dielectric material is water, most of the electromagnetic energy within the material is absorbed. Furthermore, the energy absorption ratio strongly depends on the distance of the material from the plunger end; the magnitude of its value varies approximately tenfold at most.
(5) For high water temperature at 90°C, numerical analysis predicts the influence of the dielectric position on the energy absorption ratio, which is in relatively good agreement with the results of the experiment. However, for water temperatures lower than 90°C, the present analysis overestimates the influence of the dielectric position on the energy absorption ratio.

Acknowledgements—The authors would like to express their gratitude to their former students, Mr Yasushi Kuno and Mr Toshitake Ushiwatari, for their earnest contribution in the experimental study and the development of the computer program for numerical simulation.

REFERENCES

1. Arlett, P. L., Bahrani, A. K. and Zienkiewicz, O. C., Application of finite elements to the solution of Helmholtz's equation. *Proceedings of the IEE*, 1968, **115**, 1762–1766.
2. Tompkins, D. T., Vanderby, R., Klein, S. A., Beckman, W. A., Steeves, R. A. and Paliwal, B. R., Effect of interseed spacing, tissue perfusion, thermoseed temperatures and catheters in ferromagnetic hyperthermia: results from simulations using finite element models of thermoseeds and catheters. *IEEE Transactions of Biomedical Engineering*, 1994, **41**(10), 975–985.
3. Gibson, A. A. P. and Helszajn, J., Finite element solution of longitudinally magnetized elliptical gyromagnetic waveguides. *IEEE Transactions of Microwave Theory Techniques*, 1989, **37**(6), 999–1005.
4. Radak, B. and Gluckstern, R. L., Penetration of electromagnetic fields through an elliptical hole in a wall of finite thickness. *IEEE Transactions of Microwave Theory Techniques*, 1995, **43**(1), 194–204.
5. Yee, K. S., Numerical solution of initial boundary value problems involving Maxwell's equation in isotropic media. *IEEE Transactions of Antennas Propagation*, 1966, **AP-14**(3), 302–307.
6. Smith, R. L., Iskander, M. F., Andrade, O. and Kimrey, H., Finite-difference time-domain (fdtd) simulation of microwave sintering in multimode cavities. *Microwave Processing of Materials III*, 1992, **269**, 47–52.

7. Clemens, J. and Saltiel, C., Numerical modeling of materials processing in microwave furnaces. *International Journal of Heat and Mass Transfer*, 1996, **39**(8), 1665–1675.
8. Von Hippel, A. R., *Dielectric Materials and Applications*. MIT Press, Boston, MA, 1954, p. 361.
9. Ohlsson, T., Bengtsson, N. E. and Risman, P. O., The frequency and temperature dependence of dielectric food data as determined by a cavity perturbation technique. *Journal of Microwave Power*, 1974, **9**(2), 129–145.
10. Echigo, R., Tada, S., Kuno, Y. and Yoshida, H., Heating mechanism in a microwave resonant applicator. *Proceedings of the 30th National Heat Transfer Symposium of Japan* (in Japanese), Vol. III, 1993, p. 760.